Experimental Study of Geometric Effect for Design of Multihole Cooling for Combustion Chamber Walls

B. Leger **, G. Schott *, G. Grienche *
* Turbomeca, Sce Aérothermodynamique
** Laboratoire Aquitain de Recherche en Aérothermique (Université de Pau)
c/o TURBOMECA
64511 Bordes Cedex, France
Email: bruno.leger@univ-pau.fr

Nomenclature

C	specific heat of the wall	$J.kg^{-1}$
d	diameter of the holes.	m
d_H	hydraulic diameter of the test module, cold side	m
e	wall thickness	m
F_L	luminosity factor	
h	convection coefficient	Wm^2K^{-1}
l	width of the multiholed zone	m
L	length of the multiholed zone	m
l_{opt}	optical path of the test module, hot side	
m	blowing ratio $(\rho_{tr}V_{tr})/(\rho_cV_c)$	
n	number of holes of the multiholed zone	
p	inter row distance (transverse direction)	m
P	gas pressure	Pa
Po	porosity of the wall	
Pr	Prandtl number	
Q	mass flow	$kg.s^{-1}$
r	air/fuel mixture mass ratio	
s	inter row distance (longitudinal direction)	m
S	heat exchange surface area	m^2
T	temperature	°K or °C
T_{aw}	adiabatic temperature, hot side	°K or °C
U	neuron excitation	
V	velocity	$m.s^{-1}$
UI	flux in infrared units received by the camera	
UI°	flux in infrared units emitted by a blackbody	

Greek symbols

α	angle of inclination of the holes with respect to the wall	
$\frac{\Delta P}{P}$	pressure loss between the cold side and the hot side.	%
Δt	time step	s
Δx	space between two pixels of the thermogram along the x axis	m
Δy	space between two pixels of the thermogram along the y axis	m
ε	emissivity	
Φ	radiant flux	$W.m^{-2}$
λ	thermal conductivity	$W.m^{-1}K^{-1}$
μ	dynamic viscosity	$kg.m^{-1}s^{-1}$
ρ	density of the wall	$kg.m^{-3}$
σ	Stefan constant	
τ	absorption coefficient	

Subscripts

atm	atmosphere
c	hot side (pressure = 1 atm)
ct	casing
ext	exterior
f	cold side (temperature = 300 K)
hb	porthole
jet	hole flow
tr	hole
w	wall

1. INTRODUCTION

The increase of temperature and pressure in the gas turbines is a general trend that allows the engine performances to be increased. These higher thermodynamic cycles impose cooling systems of increasingly high performance. As a matter of fact, lean combustion, that is necessary to reduce the amount of nitrogen oxides (Nox) produced, consumes more and more air, and this air is taken mainly from the air usually reserved for cooling. The decrease of the quantity of air available for the cooling systems and the increase of the gas temperature in the combustion chamber are contradictory elements of the problem which oblige us to better control wall temperatures with a minimum air consumption.

Multiholed walls in combustion chambers remain a satisfactory, efficient and low-cost solution to the problem. We have designed a test cell which allows us to improve our knowledge of this type of cooling system by varying the aerothermodynamic and geometric parameters [1]. Many studies have been conducted on a single hole [2,3] or on one, two or three rows of holes [4,5]. These fairly complete studies well show the aerodynamic (jet penetration, turbulence analysis) and thermal (localized increase of heat transfer in and around the hole) aspects, but are in most cases applicable to the cooling of turbine

Paper presented at the RTO AVT Symposium on "Advanced Flow Management: Part B – Heat Transfer and Cooling in Propulsion and Power Systems", held in Loen, Norway, 7-11 May 2001, and published in RTO-MP-069(I).

Report Documentation Page

Form Approved
OMB No. 0704-0188

1. REPORT DATE	2. REPORT TYPE	3. DATES COVERED
00 MAR 2003	**N/A**	**-**

4. TITLE AND SUBTITLE	5a. CONTRACT NUMBER
Experimental Study of Geometric Effect for Design of Multihole Cooling for Combustion Chamber Walls	5b. GRANT NUMBER
	5c. PROGRAM ELEMENT NUMBER
6. AUTHOR(S)	5d. PROJECT NUMBER
	5e. TASK NUMBER
	5f. WORK UNIT NUMBER
7. PERFORMING ORGANIZATION NAME(S) AND ADDRESS(ES) **NATO Research and Technology Organisation BP 25, 7 Rue Ancelle, F-92201 Neuilly-Sue-Seine Cedex, France**	8. PERFORMING ORGANIZATION REPORT NUMBER
9. SPONSORING/MONITORING AGENCY NAME(S) AND ADDRESS(ES)	10. SPONSOR/MONITOR'S ACRONYM(S)
	11. SPONSOR/MONITOR'S REPORT NUMBER(S)

12. DISTRIBUTION/AVAILABILITY STATEMENT
Approved for public release, distribution unlimited

13. SUPPLEMENTARY NOTES
Also see ADM001490, presented at RTO Applied Vehicle Technology Panel (AVT) Symposium held in Leon, Norway on 7-11 May 2001, The original document contains color images.

14. ABSTRACT

15. SUBJECT TERMS

16. SECURITY CLASSIFICATION OF:			17. LIMITATION OF ABSTRACT	18. NUMBER OF PAGES	19a. NAME OF RESPONSIBLE PERSON
a. REPORT	b. ABSTRACT	c. THIS PAGE			
unclassified	**unclassified**	**unclassified**	**UU**	**10**	

vanes where the blowing ratio is low (m ≈ 2) compared with those found in multiholed combustion chamber walls (m ≈ 3 to 5).

Our experimental study concerns plate shapes encountered in combustion chambers at scale 1 in a realistic aerodynamic and thermal environment. Some studies on this type of surface exist but were conducted at different scales [6], at lower temperature levels [7] or also using a different mode of supply of the holes [8]. In our case, the cooling air does not completely flow across the holes (see *figure 1*), which corresponds exactly to the type of air flow encountered in combustion chambers. We have carried out a number of tests in order to determine the influence of the parameters, shown in *figure 2*, on the cooling of the multiholed wall. The use of neural networks emerged naturally, compared with traditional correlation methods, due to the multiplicity of tests and the large number of parameters considered. This constitutes a specific use of the neural networks which are usually reserved for problems such as command control or character recognition.

The geometric and aerothermodynamic parameters under study vary as follows:

geometric parameters:	aerothermodynamic parameters:
$20 < \alpha < 120$ ° ; $0.3 < d < 0.7$ mm ; $1.025 < p < 1.685$ mm ; $0.905 < s < 4.03$ mm.	$0.5 < \Delta P/P < 12$ % ; $600 < Tc < 1400$ K ; $10 < Qf < 400$ g/s ; $35 < Qc < 500$ g/s.

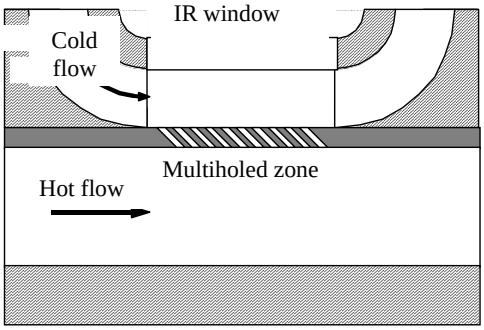

Figure 1. Test module.

The experimental study has been conducted on 18 plates of different shape, selected so as to enable each of the geometric parameters (angle and diameter of the holes, transverse and longitudinal pitch) to be studied separately. For each plate, we have studied 33 specific aerothermodynamic conditions selected in order to scan the aerothermodynamic characteristics encountered in the combustion chambers of gas turbines.

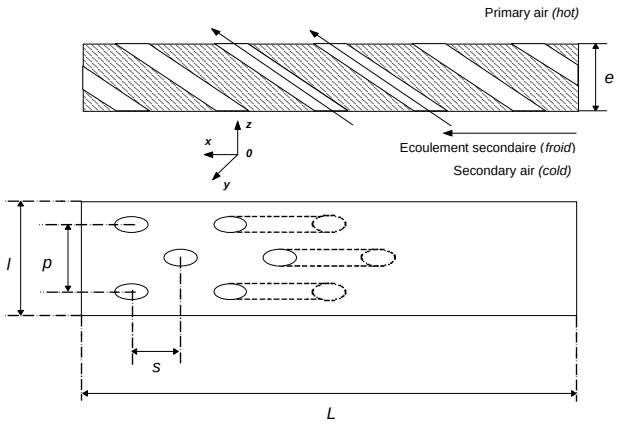

Figure 2. Geometric parameters.

The measurements were made using an infrared camera. Our problem can be represented schematically, as shown in *figure 3*, by assuming that we aim at an object under a temperature T_0, in a given environment, and this through an IR porthole and a gaseous atmosphere.

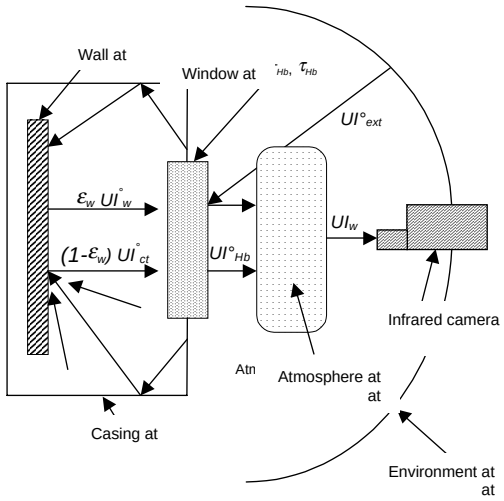

Figure 3. Schematic representation of the IR measurement problem.

If we call the radiometric flux measured by the infrared camera Φ_m, we may write:

$$\Phi_m = \tau_h \left[\underbrace{\tau_{atm}\,\varepsilon_0\,\Phi(T_0)}_{wall} + \underbrace{\tau_{atm}\,\rho_0\,\Phi(T_e)}_{environment} + \underbrace{\tau_{atm}\,\tau_0\,\Phi(T_f)}_{bottom} + \underbrace{(1-\tau_{atm})\,\Phi(T_{atm})}_{atmosphere} \right] + \underbrace{(1-\tau_h)\,\Phi(T_h)}_{window}$$

On our thermograms, processed and stored in the form of computer files, we may see the cooling of the plate obtained as a result of the presence of the multiple holes.

Since our aim is to define correlations that can be used to presize the cooling system of the combustion chamber walls, we have tried to synthesize all the measurement results by making a global modelling of the multihole cooling system.

2. THERMAL MODELING:

2.1. Flux balance:

The flux balance of the multiholed plate applied to a pixel of the infrared image having the co-ordinates (x, y) is written using the following equation of energy:

$$\rho_w C_w \frac{\partial T_w(x,y,z,t)}{\partial t} = \lambda_w \left(\frac{\partial^2 T_w(x,y,z,t)}{\partial x^2} + \frac{\partial^2 T_w(x,y,z,t)}{\partial y^2} + \frac{\partial^2 T_w(x,y,z,t)}{\partial z^2} \right)$$

The plate thickness is 0.8 mm. It may therefore be considered as thin: the temperature gradient along z is thus considered to be zero.

Which allows us to write:

$$\rho_w C_w e \frac{\partial T_w(x,y,0,t)}{\partial t} = \phi_{cd,x} + \phi_{cd,y} + \phi_{cv,c} + \phi_{ray,c} - \phi_{cv,f} - \phi_{ray,f} - \phi_{cv,tr}$$

where:

- $\phi_{cd,x}$: density of heat flow rate transferred by conduction along x through the wall;
- $\phi_{cd,y}$: density of heat flow rate transferred by conduction along y through the wall;
- $\phi_{cv,c}$: density of heat flow rate transferred by convection of the burnt gases towards the wall;
- $\phi_{ray,c}$: density of heat flow rate transferred by radiation of the burnt gases and the hot casings towards the wall;
- $\phi_{cv,f}$: density of heat flow rate emitted by convection from the wall towards the cooling gases;
- $\phi_{ray,f}$: density of heat flow rate emitted by radiation from the wall towards the cold casings and the porthole;
- $\phi_{cv,tr}$: density of heat flow rate emitted by convection towards the cooling gases flowing across the holes of the multiholed zone.

$\phi_{cd,x}$, $\phi_{cd,y}$, $\phi_{ray,c}$, $\phi_{cv,f}$ and $\phi_{ray,f}$ are modeled using a conventional method: finite differences, radiation according to the usual formulation and convection coefficient according to Colburn. The convection flux in the holes follows the Colburn formulation taking into account the relative surface area of the hole with respect to the plate.

$$\Phi_{cv,tr} = \xi_{tr} h_{tr}(x,y)\left[T_w(x,y,0,t) - T_f(x,y)\right]\left(\frac{\pi d\, e}{\sin\alpha}\right)\left(\Delta x\,\Delta y - \frac{\pi d^2}{4\sin\alpha}\right)^{-1}$$

where:

- $h_{tr}(x, y)$ according to Colburn;
- $\xi_{tr} = 0$: the pixel has no multiholed plate hole;
- $\xi_{tr} = 1$: the pixel has a multiholed plate hole.

Using the equations of the flux balance written in transient mode (the temperature of the hot gases rises briefly, which causes the plate temperature to rise) and in steady-state mode allows us to calculate h_c and T_{aw}, the only unknowns of the problem, related by the relation $\phi_{cv,c} = h_c(x,y)\left[T_{aw}(x,y) - T_w(x,y,0,t)\right]$, according to a method based on J. Descoins' method [9].

This method is applied to all of our experimental cases, which allows us to know h_c and T_{aw} profiles for each aerothermodynamic condition corresponding to a test.

2.2. Modeling h_c and T_{aw}:

Knowing h_c and T_{aw}, it remains for us to model them in order to predict wall temperatures using the flux balance. We build this model from all our experimental results. The relative influence of h_c on the calculated wall temperature value is far less than the T_{aw} value. For this reason, we have modeled h_c using a simple method (see *figure 4*) and have given our attention to T_{aw}.

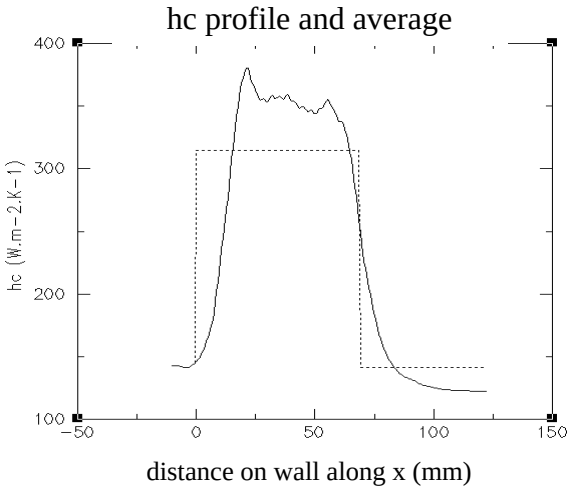

Figure 4. Experimental profile of h_c and value modeled in the multiholed zone.

The *figure 5* shows 4 longitudinal profiles of convection coefficients, on the hot side, obtained from the IR measurements and calculated from the flux balance. These profiles were obtained during 4 tests corresponding to 4 different aerothermodynamic conditions conducted on a same plate and show how difficult it is to model h_c.

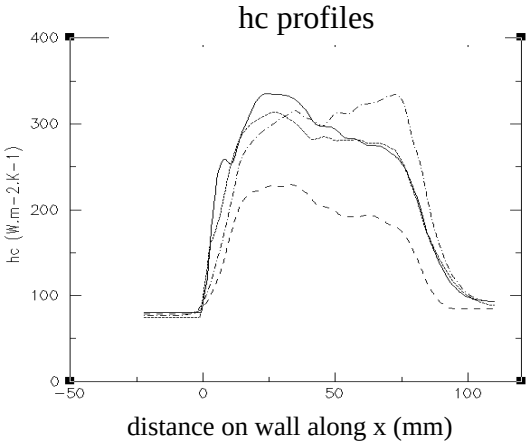

Figure 5. Longitudinal profiles of h_c.

We observe a large variety of profiles of convection coefficients on the hot side and we have therefore chosen to model the difference Δh between the average value of h_c calculated in the multiholed zone (see figure 4) and the value of h calculated according to Colburn corresponding to the value in the zone located upstream of the multiholed zone, as follows:

$$\Delta h = 165(1 - e^{-100x^{0.95}})$$

where :

- $x = \rho_{jet} \times V_{jet} \times Po \times L^2$;
- $\rho_{jet} = \rho_f \left(\frac{P_c}{P_f} \right)^{\frac{1}{\gamma}}$;
- $V_{jet} = \sqrt{\frac{2\Delta P}{\rho_{jet}}}$;
- $Po = \frac{n \times \pi \times d^2}{4} \ / \ (L \times l)$.

Each calculated adiabatic temperature is modeled from the adiabatic efficiency $\eta_{aw} = \frac{T_c - T_{aw}}{T_c - T_f}$ according to a mathematical formulation in which 8 coefficients are used. The abscissa x and the length of the multiholed zone are dimensionless in x* and L* in accordance with reference values.

Mathematical formulation of the adiabatic efficiency modeling:

- For $x^* \le L^*$ (in the multiholed zone)

$$\eta_{aw}(x^*) = (1 - \eta_u)\left(1 - \exp\left[-\frac{x^* + 44{,}604}{2000 C_1}\right]\right)^{C_2}\left(1 - \frac{C_4^2}{\left(\frac{x^* + 44{,}604}{2000}\right)^{C_3^2} + C_4^2}\right) + \eta_u$$

- For $x^* > L^*$ (downstream of the multiholed zone)

$$\eta_{aw}(x^*) = (\eta_d - \eta_e)\left(1 - \exp\left[-\frac{x^* - L^*}{2000\ C_5}\right]\right)^{C_6} + \eta_e$$

Where:

- η_u : adiabatic efficiency upstream of the multiholed zone (*upstream zone*). Although its value is zero in theory (*in this case the wall is solid and the adiabatic temperature is equal to the temperature of the hot gases:* $T_{aw} = T_c$), we admit a value slightly different from zero in order to compensate for the errors due to the convective – radiative transfer models used.

- η_e : adiabatic efficiency at the end of the multiholed zone (*end zone*), given by the following relation: $\eta_e = \eta_{aw}(x^* = L^*)$. It represents the maximum adiabatic efficiency value.

- η_d : adiabatic efficiency downstream of the multiholed zone (*downstream zone*) given by the following relation: $\eta_d = (1 - |\Delta\eta_d|)\eta_e$

For each test case, the coefficients $C_{i=1,6}$ as well as the η_u and $\Delta\eta_d$ values are calculated using the Nelder Mead's method of the simplex which calculates the 8 coefficients of the adiabatic efficiency curve whose corresponding wall temperature curve is the closest to that obtained with the infrared camera.

The *figure 6* shows the relevance of adiabatic temperature mathematical modelling using the 8 coefficients.

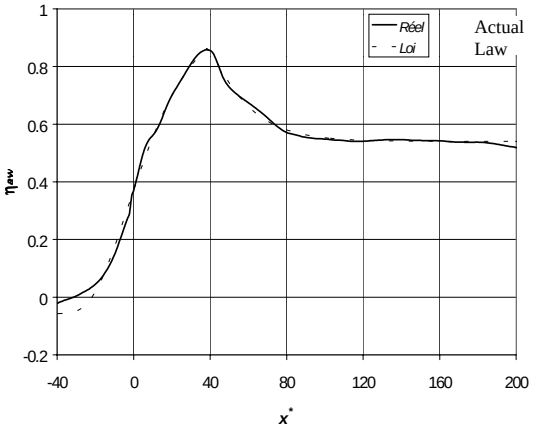

Figure 6. Actual and modeled adiabatic efficiencies.

These 8 coefficients depend on the geometric and aerothermodynamic parameters and are calculated for each test using Nelder Mead's solver, and working therefore in a space of 8 dimensions. The progression of the solver is achieved by reducing progressively the difference between the actual temperature of the plate and the temperature simulated from the flux balance where the only unknown is the plate temperature. At each iteration, a simulation is thus calculated from the corresponding 8 coefficients.

In order to simulate a plate temperature, we have therefore to build a model with the 8 coefficients. Due to the complexity of a mathematical formulation of the 8 coefficients from geometric and aerothermodynamic parameters, we have moved towards the use of neural networks. In fact, neural networks are capable of interpolating complex functions, without mathematical formulation. After a so-called learning phase, we may integrate them into modules of existing software programs (in this case the program we have written for calculating the wall temperatures), which allows the problems to be handled in cases where conventional data processing systems are too weak [10]. We therefore use 8 neural networks, one for each coefficient to be simulated.

3. INTRODUCTION TO NEURAL NETWORKS:

3.1. The formal neuron:

A neuron can be described as a small decision-making automaton. It consists of 2 parts having the following distinct functions:

- evaluation of the stimuli received;
- evaluation of its internal state.

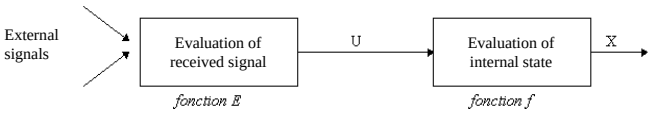

Figure 7. Formal neuron diagram.

A neuron is therefore characterized by:

- its state (X) ;
- the excitation level received at its input (U) ;
- its transition function f ;
- its input function E (a sum in general).

3.2. The interconnections:

The interconnection topology of the neural networks can be extremely varied. Several types of networks can be created simply by modifying the interconnection rules. The singularity of the interconnection is to be weighted. This allows the relationship between the neurons, i.e. the influence of the activation of a neuron on another neuron, to be simulated.

In most cases, the connections serve to calculate the input of the neuron whereas the activation functions determine the output.

3.3. Mc Culloch and Pitts' neuron – the multilayer perceptron:

The first definition of the neuron, that of Mc Culloch and Pitts, dates from 1943.

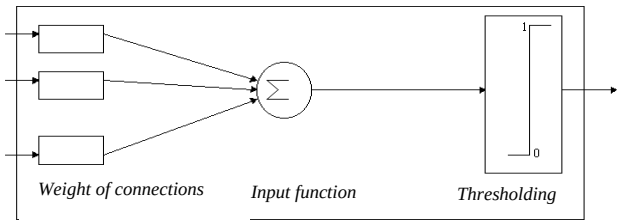

Figure 8. Mc Culloch and Pitts' neuron.

Therefore, the input function can be calculated very easily: $U_i = \sum_{j=1}^{n} W_{ij} \cdot x_j$ where:

- W_{ij} is the weight of the interconnection between the n upstream neurons j and the downstream neuron i;
- x_j is the excitation of upstream neuron j;
- U_i is the input of the neuron being considered.

The activation of the neuron is therefore given simply by $x_i = f(U_i)$. In our case, f is not the thresholding function but the sigmoid function $x_i = f(U_i) = \frac{1}{1+e^{-U_i}}$, which is typically used in scenarii like ours and which is close to the thresholding function.

The network presented herein, the multilayer perceptron (see *figure 9*) which is the most appropriate to the study of our problem, has the following characteristics:

- a single input layer;
- a single output layer;
- it may contain one or more hidden layers;
- each neuron is only connected to all the neurons of the next layer.

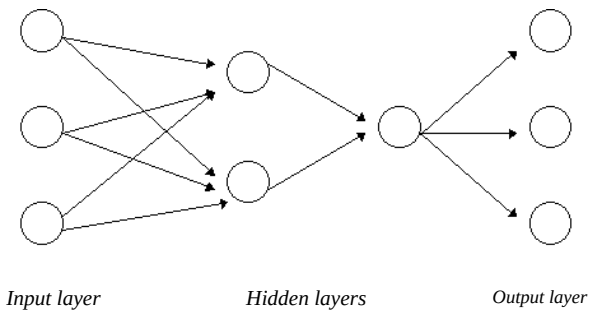

Figure 9. Example of multilayer perceptron.

Although this type of model reproduces faithfully the biological neuron, its implementation implies that the weights associated with the connections are known. A so-called learning phase must therefore be applied to the network to set the weights of the connections.

3.4. The learning phase:

In order that the network performs the best interpolation, inputs are transmitted to the network and the network is requested to modify its weights to obtain the corresponding outputs. The outputs in question are obtained from the Nelder Mead's solver applied to our test conditions. The algorithm consists in first propagating the inputs forwards until an output calculated by the network is obtained. The second step compares the calculated output with the known actual output. The weights are then modified so that, when the next iteration is performed, the error made between the calculated output and the known output is minimized. Nevertheless, hidden layers shall not be forgotten. For this reason, the error made is propagated backwards up to the input layer while the weights are being modified. This process is repeated on all the examples until an output error considered to be negligible is obtained.

We have used the software program SNNS from the University of Stuttgart to manage all neural network issues. The software, quite user friendly, enables the user to create a network geometry, perform the learning phase (several algorithms are available) then use the network for function interpolation [11].

4. USING THE NEURAL NETWORKS:

4.1. Inputs:

As explained above, each of our 8 neural networks have 4 inputs corresponding to 4 aerothermodynamic parameters, $\Delta P / P$, $\rho_c V_c$, $\rho_f V_f$ and $\frac{T_c}{T_f}$, and one output, the modeled coefficient. Each input and output is maintained within the interval [0,1] in which the network works for numerical reasons by using the corresponding minimum and maximum values as follows: $x_{[0,1]} = \frac{x - x_{\min}}{x_{\max} - x_{\min}}$.

Thus, this enables a plate of given shape to be modeled. The possibility of modeling all the shapes and aerothermodynamic conditions may be envisaged by adding geometric parameters to the inputs of the neural networks.

4.2. Geometry of hidden layers:

One of the crucial problems of using the neural networks in good conditions, is the number of hidden layers as well as the number of neurons on each layer. If the number of neurons is too low, the learning phase will not converge, the network will have two many data to learn and not enough neurons to store them: the network will tend to underfit the interpolations; it is not enough intelligent. On the contrary, if the number of neurons is too high, the network will converge rapidly but the interpolated points, excluding the points learnt, will be completely false: then there will be overfitting: the network is too intelligent.

In order to compare the effectiveness of the different networks, we have performed so-called propagation phases which consist, after the learning phase has been completed on a given known function, in propagating forwards the input values across the network so as to calculate the output values and to compare them with the given known function.

5. RESULTS

The *figure 10* gives the results of the simulation per neural network of a plate temperature profile as well as the corresponding adiabatic efficiency on a case which was not used for learning.

The plate temperatures measured by infrared thermography and the simulation results are very close, in particular in the case of the two important parameters which characterize the cooling system: the minimum temperature reached and the gradient along the plate.

Therefore, we observe the ability of our model to predict the temperature of multiholed flat plates placed between two given flows and whose geometric and aerothermal parameters are part of our field of study.

Similarly, we observe the efficiency of the solution given by the neural networks to a problem like ours, when a mathematical formulation seems difficult to write in the form of a correlation.

The unknowns of our problem, h_c and $T_{aw,}$ are then represented by the two parameters used in the formulation of Δh and by the 8 neural networks which provide us with an adiabatic efficiency curve.

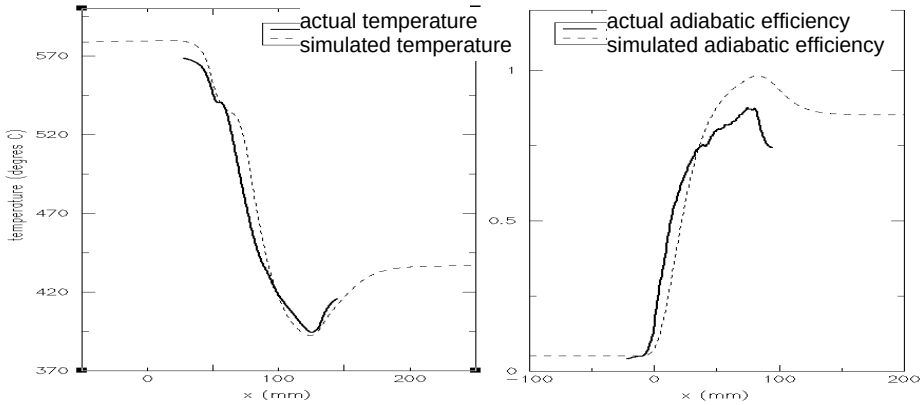

Figure 10. Simulation of the temperature of a plate not used in the learning process

On figure 11 below, we present a typical measurement and a comparison with the calculation. We can observe the cooling effect within the multiholed zone and its prolongation after this zone. The film cooling created after the multiholed zone is very interesting because there is no air consumption to protect the wall.

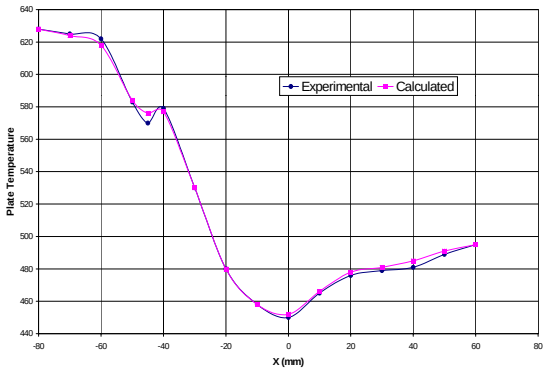

Figure 11: Temperature measurement along a multiholed plate

The figure 12 shows different temperature profile along a multiholed plate with different diameter of holes. Of course the gradients are greater when the diameter increase but the air consumption is increasing too. We can observe that 0.5 mm diameter is a good compromise and avoid an augmentation of the temperature given by lower diameter in the first rows.

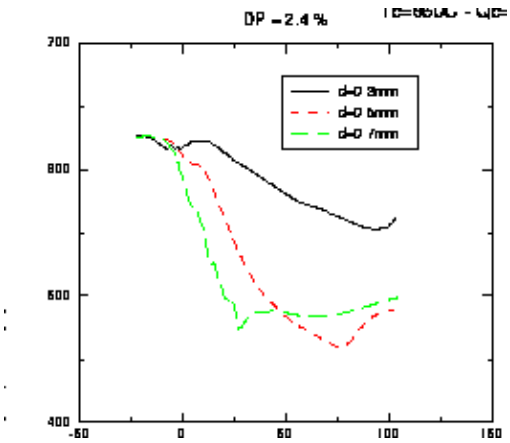

Figure 12: diameter influence on the temperature profile

The influence of the longitudinal pitch is given figure 13 below. When the pitch decreases, the air consumption and the gradient of the temperature profile increase. A combination of the longitudinal pitch and the hole diameter is interesting to do, in order to control the cooling effect and the air consumption.

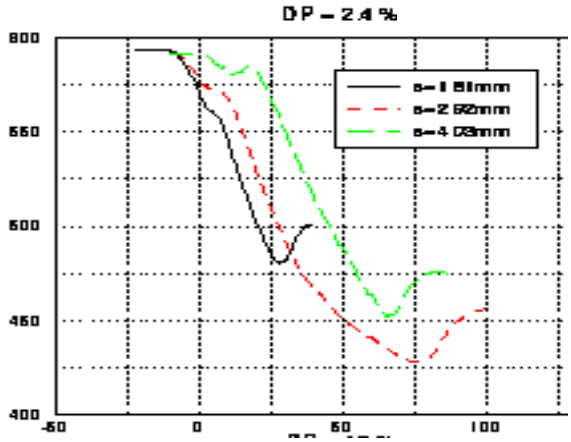

Figure 13: longitudital pitch influence

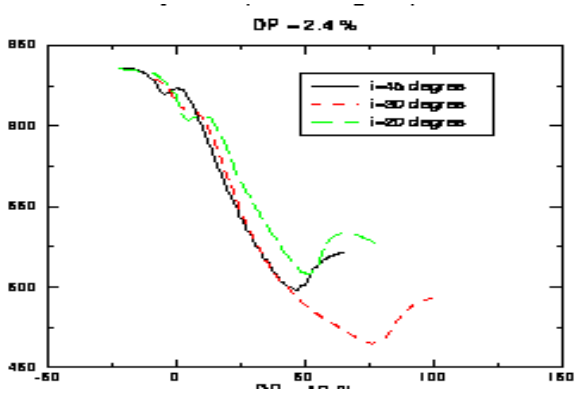

Figure 14: Hole angle effect

On figure 14, is given the influence of the hole angle. It is surprising to see that the hole angle has no determinant influence on the cooling effect within the multiholed zone. This means that the heat transfer by convection in the holes is not significant regarding the wall protection. The more important characteristic to protect the combustion chamber wall is the development of a film

cooling along the plate that preserves this wall from the hot gases

6. CONCLUSIONS

We have used the flux balance in a reverse way: knowing all the fluxes, with h_c modeled by the relation $\Delta h = 165(1 - e^{-100x^{0.95}})$ and T_{aw} obtained via neural networks, the only unknown of the problem is the plate temperature. It can therefore be calculated.

Thus, a plate temperature profile can be simulated for an aerothermodynamic case, provided that they are part of the field of study of the parameters of the problem, the field of study in which the neural network is capable of making an interpolation of an adiabatic efficiency.
This study was extended to the influence of he geometric characteristics of the multihole cooling device which are the hole diameter, the longitudinal pitch and the hole angles. We have measured these influences, and this gives us the ability to control the temperature gradient and the air consumption for a numerous different design of multihole cooling.
.

REFERENCES

[1] Léger B., André P., Grienche G. et Schott G. *Contrôle thermique de parois de chambre de combustion. Banc d'essai du Laboratoire Aquitain de Recherche en Aérothermique*. Revue générale de thermique, 35, pages 625 à 630, Septembre 1996.

[2] Le Grives E., Nicolas J.J. et Genot J. Internal Aerodynamics and heat transfer problem associated to film cooling of gaz turbines. ASME n° 79, GT 57, 1979.

[3] Fric T.F. et Roshko A., *Vortical structures in the wake of a tranverse jet*, J.Fluid Mech., vol.279, pp.1-47, 1994.

[4] Bousgarbies J.L., Bernard A., Brizzi L.E., Dorignac E., Vullierme J.J., *Ecoulement au voisinage d'une paroi plane soumise à l'impact d'un ensemble de jets : application au refroidissement de paroi*. Revue Française de Mécanique, Vol.2, pp.99-103, 1996.

[5] Brown A. et Saluja C.L. *Film cooling from three rows of holes on adiabatic constant heat flux and isothermal surfaces in the presence of variable freestream velocity gradient and turbulence intensity*. ASME n° 79, GT 24, 1979.

[6] Andrews G.E., Alikhanizadeh M., Asere A.A., Hussain C.I., Khoshkbar Azari M.S. et Mkpadi M.C. *Small diameter film cooling holes : Wall convective heat transfer*. ASME n° 86, GT 225, 1986.

[7] M. Martiny, A. Schulz et S. Wittig. *Mathematical model describing the coupled heat transfer in effusion cooled combustor wall*. ASME n° 97, GT 329, Juin 1997.

[8] Champion J.L., Dorignac E. et Deshaies B. *Etude expérimentale du processus de refroidissement d'une plaque multiperforée*. Congrès sur la thermique de l'homme et de son proche environnement, Société Française des Thermiciens, pages 254 à 259, Mai 1995.

[9] Descoins J. *Caractérisation de techniques de refroidissement de paroi : application de la thermographie infrarouge au cas du soufflage pariétal*. Thèse de doctorat, Ecole Nationale Supérieure de l'Aéronautique et de l'Espace, Janvier 1991.

[10] Dreyfus G. *Les réseaux de neurones*. Les applications des réseaux de neurones à la mécanique – CETIM, décembre 1997.

[11] Stuttgart University. *Logiciel de réseau de neurones SNNS*.
ftp://ftp.informatik.uni_stuttgart.de/pub/

Paper Number: 10

Name of Discusser: B. Simon, MTU Aero Engines Munich

Question:
You detected no influence of inclination on wall temperature. I would conclude that effusion holes were to narrow spaced.

Answer:
The experiments were done with high blowing ratio (2 to 5 or more). I suppose the result would not be the same for lower blowing ratios, but we observed that this is no significant effect due to the augmentation of the hole surface because of the inclination. Perhaps there is a saturation of the cooling effect in the holes due to the high blowing ratio.

Name of Discusser: H. Weyer, DLR Cologne

Question:
Did you care of the effect of flow properties on the “cold side” on the heat transfer?

Answer:
Our test facility don’t allow us to change the properties of the cold air
This cold air have ambient properties atmospheric pressure.

This page has been deliberately left blank

Page intentionnellement blanche